Int. J. Solids Structures Vol. 24, No. 7, pp. 683–703, 1988
Printed in Great Britain.

0020–7683/88 $3.00 + .00

THREE-DIMENSIONAL ELASTIC ANALYSIS OF CRACKED THICK PLATES UNDER BENDING FIELDS

K. T. SUNDARA RAJA IYENGAR
Department of Civil Engineering, Indian Institute of Science, Bangalore 560 012, India

and

M. V. V. MURTHY and M. N. BAPU RAO
Structures Division, National Aeronautical Laboratory, Bangalore 560 017, India

(*Received* 19 *February* 1987; *in revised form* 30 *December* 1987)

Abstract—A three-dimensional analysis is presented for the bending problem of finite thick plates with through-the-thickness cracks. A general solution is obtained for Navier's equations of the theory of elasticity. It is found that the in-plane stresses and the transverse normal stress at the crack front are singular with an inverse square root singularity, while the transverse shear stresses are of the order of unity. Results from a numerical study indicate that the stress intensity factor, which varies across the thickness, is influenced by the thickness ratio in a significant manner. Results from a parametric study and those from a comparative study with existing finite element values are presented.

NOTATION

$2a$	crack length
E	Young's modulus
G	rigidity modulus
$I_n(A), K_n(A)$	modified Bessel functions of the first and second kind, respectively
$K_b(\bar{Z})$	stress intensity factor (commonly referred to as SIF), expressed as a function of the coordinate in the thickness direction, i.e. $\bar{Z}$
$\overset{*}{K}_b(\bar{Z})$	factor associated with the singular part of the normal stress component along the thickness direction, analogous to $K_b(\bar{Z})$
$2L, 2B, 2h$	length, breadth and thickness of the plate (Fig. 1)
M_0	applied bending loading
n	defined under four different groups as: (i) $n = 2j + 1/2$, (ii) $n = 2j - 1/2$, (iii) $n = 2j + 1$, (iv) $n = 2j$, with $j = 0, 1, 2, 3, \ldots, \infty$
Q_x, Q_y M_x, M_y, M_{xy}	stress resultants and couples in the Cartesian coordinate system
$\bar{r}, \theta, \bar{Z}$	cylindrical coordinate system, associated with the Cartesian coordinate system such that the relations $\bar{X} = \bar{r}\cos\theta$, $\bar{Y} = \bar{r}\sin\theta$ and $\bar{Z} = \bar{Z}$ are valid (Fig. 2)
u, v, w	non-dimensionalized displacement components in the cylindrical coordinate system where $(u, v, w) = (\bar{u}/a, \bar{v}/a, \bar{w}/a)$
$\bar{u}, \bar{v}, \bar{w}$	displacement components in the cylindrical coordinate system
X, Y, ζ r, θ, ζ	non-dimensionalized Cartesian and cylindrical coordinate systems where $(X, Y, \zeta) = (\bar{X}/a, \bar{Y}/a, \bar{Z}/a)$ and $(r, \theta, \zeta) = (\bar{r}/a, \theta, \bar{Z}/a)$
$\overset{\circ}{X}, \overset{\circ}{Y}, \overset{\circ}{Z}$	Cartesian coordinate system with the origin at the centre of the plate (Fig. 1)
$\bar{X}, \bar{Y}, \bar{Z}$	Cartesian coordinate system with the origin at the crack front such that $-h \leqslant Z \leqslant h$ (Fig. 2)
$(\,)'$	partial derivative with respect to ζ, $\partial/\partial\zeta$.

Greek symbols

α, β	partial derivatives, $\partial/\partial r$, $1/r\,\partial/\partial\theta$, respectively
γ_l	real roots, $l'\pi$ where $l' = l + 1/2$, $l = 0, 1, 2, \ldots, \infty$
η	thickness parameter, h/a
λ_k, ω_k	complex roots, with $k = 1, 2, 3, \ldots, \infty$
μ	Poisson's ratio
ρ	dilatation
σ_b	extreme fibre stress due to applied bending loading, $3M_0/2h^2$
$\sigma_r, \sigma_\theta, \sigma_z$ $\sigma_{r\theta}, \sigma_{rz}, \sigma_{\theta z}$	stress components in the cylindrical coordinate system
$\sigma_x, \sigma_y, \sigma_z$ $\sigma_{xy}, \sigma_{xz}, \sigma_{yz}$	stress components in the Cartesian coordinate system
χ, ψ, Ω	stress functions.

INTRODUCTION

It is well known that the state of stress in the neighbourhood of the crack front in a cracked plate of finite thickness is three-dimensional in nature. It is, therefore, essential that a three-dimensional analysis is carried out in order to understand the true behaviour of the stress and deformation fields prevailing in the vicinity of the crack front.

Among various crack configurations encountered in practice, the through-the-thickness crack configuration is of particular interest. Recent studies[1–4] in cracked-plate problems with through-crack geometry have raised some questions such as (i) the type of stress singularities involved at the crack front, in particular at the corner points where the crack front penetrates the free plate faces, (ii) the type of variation of the stress intensity factor (SIF) across the plate thickness, in particular near the plate faces and (iii) the character of the displacement field prevailing at the crack front. These studies point to the existence of the inverse square root singularity $1/\sqrt{r}$ (where r is the radial distance from the crack front) in the stress field interior to the plate thickness with a predominantly plane strain type of deformation field. However, near the plate faces, while Refs [1, 2] do not shed any light as to either the type of stress singularity or the deformation character, the studies in Refs [3, 4] reveal a Poisson's ratio-dependent (μ) stress singularity, namely $1/(r)^{1.2+2\mu}$, indicating a displacement singularity at the crack front for $\mu > 1/4$. In contrast, in Refs [1, 2], the condition of finiteness of displacement components at the crack front is enforced on the solution. At this point it may be mentioned that the above-mentioned studies[1–4] are qualitative in nature since no numerical studies have been carried out. The experimental studies carried out by Villarreal *et al.*[5] serve to confirm the qualitative results presented in Refs [1–4] regarding the character of the singular deformation field interior to the plate thickness, but, near the plate faces, the results obtained in this paper indicate a rapid decrease in SIF values, thereby suggesting a reduction in the strength of the singularity in the region.

More recently, an analytical solution[6] was presented for the three-dimensional stress problem of a finite thick plate with a through-the-thickness crack under an extensional loading. A general solution to the Navier equation was obtained, which revealed that the in-plane stresses and the transverse normal stress at the crack front were singular with an inverse square root singularity, while the transverse shear stresses were of the order of unity. The stress intensity factor, which varied with the coordinate in the thickness direction, was found to depend, predominantly, on the thickness ratio of the plate. The in-plane stresses preserved the inverse square root singularity all through the plate thickness including the corner points where the crack front penetrates the faces of the plate. The displacement components at the crack front were finite; in fact, this condition was imposed on the solution solely from physical considerations. Numerical results were obtained for the SIF for some typical problems. It was found that in the region interior to the plate thickness the SIF had a character, more or less that of plane strain, particularly for large thickness ratios, and for the case with $2h \to \infty$ (where $2h$ is the plate thickness), the two-dimensional plane strain solution was mathematically recovered. For particular cases, the results for the SIF applicable for the region interior to the plate thickness were found to be in good agreement with those of the finite element method[7] and the experimental method[5]. The numerical results for the SIF valid for other regions across the plate thickness exhibited significant features, not observed before in earlier investigations.

The above-mentioned investigations deal with extensional loading problems only, in which the deformation field about the plate middle plane is symmetric. Crack problems associated with the antisymmetric deformation field about the plate middle plane are also important, since the solution for general loading cases, which are frequently encountered in practice, requires consideration of both symmetric and antisymmetric fields. A study of the existing literature reveals that three-dimensional results obtained from analytical methods for the antisymmetric problems are not available. In this connection, it may be mentioned here that the studies carried out by Hartranft and Sih[8] are found to be two-dimensional in nature for cracked plate problems involving stress-free plate faces. However, some results obtained by the finite element and photoelastic methods are available[9–12].

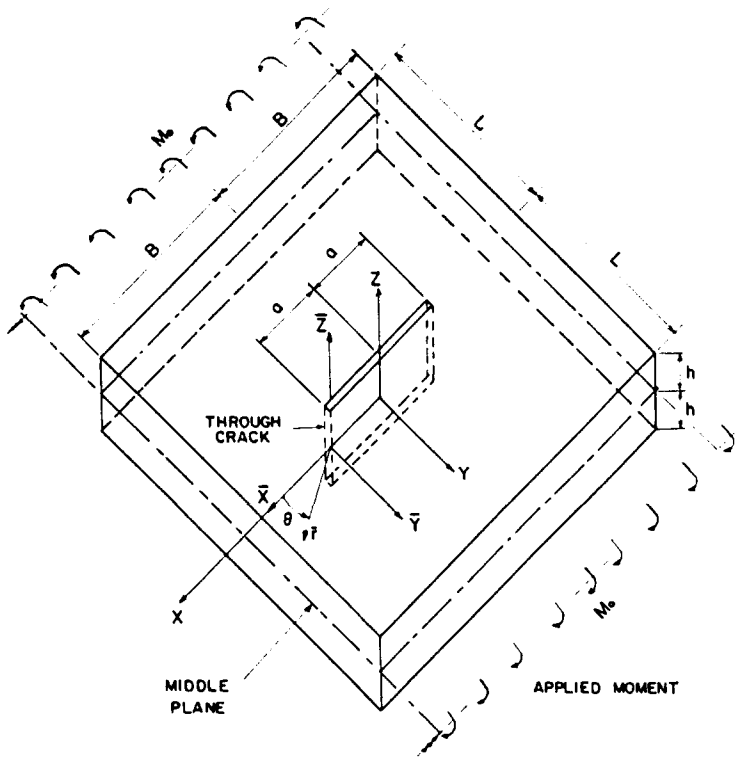

Fig. 1. Coordinate system and plate dimensions (bending loading case).

Thus, a need for undertaking the three-dimensional analysis using exact theoretical methods is clearly indicated for crack problems involving antisymmetric deformation fields, where the stress intensity factor varies in an antisymmetric manner with respect to the plate middle plane.

In this paper, a three-dimensional elastic analysis is presented for the bending problem of finite rectangular thick plates with through-the-thickness cracks. The mathematical formulation is developed using the equations of the theory of elasticity[13, 14]. A general solution is obtained, which satisfies exactly the stress-free boundary conditions at the crack surfaces and the plate faces. The solution also satisfies the boundary conditions at the exterior (outer) edges of the plate, which include those associated with the applied loading, in the least square sense. Numerical studies have been carried out for the loading case involving the application of the uniform unidirectional moment at the exterior plate edges which are parallel to the crack plane. The effect of various parameters of the problem, in particular the thickness ratio, on the stress intensity factor has been determined. Some of the results have also been compared with existing results from the finite element method. The nature of the present results and those of the comparison study have led to some interesting conclusions.

FORMULATION OF THE PROBLEM

The problem to be analysed here is that of the bending of a rectangular plate with a length of $2L$, a width of $2B$ and a thickness equal to $2h$, containing a central through-the-thickness crack of length $2a$ (Fig. 1). The plate is subjected to a uniformal uniaxial bending moment M_0 at the outer edges, which are parallel to the crack plane.

The plate bending problem described above involves a deformation character which is antisymmetric with respect to the middle plane of the plate, that is, the $\dot{X}$–$\dot{Y}$ plane. Specifically, the in-plane displacements as well as the in-plane stresses (associated with the $\dot{X}$- and $\dot{Y}$-directions) and the transverse normal stress (along the $\dot{Z}$-axis) are antisymmetric with

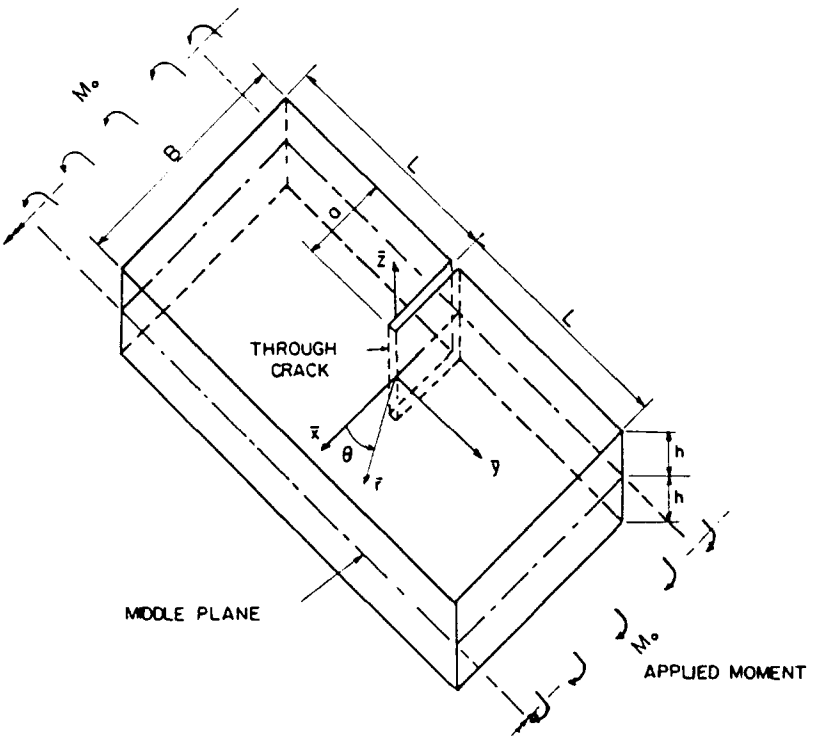

Fig. 2. Plate of finite dimensions with a through-the-thickness crack under uniform bending loading.

respect to the middle plane, while the transverse displacement and transverse shear stresses are found to be symmetric with respect to this plane. In developing the mathematical formulation of the problem the foregoing factors concerning the character of the stress and displacement distributions across the plate thickness must be taken into account.

LOCAL COORDINATE SYSTEM

In a Cartesian coordinate system $(\dot{X}, \dot{Y}, \dot{Z})$ with the origin located at the centre of the plate middle plane such that $-B \leqslant \dot{X} \leqslant B$, $-L \leqslant \dot{Y} \leqslant L$ and $-h \leqslant \dot{Z} \leqslant h$ (Fig. 1), the crack occupies a region defined by $-a \leqslant \dot{X} \leqslant a$, $\dot{Y} = \pm 0$ and $-h \leqslant \dot{Z} \leqslant h$. For convenience, the general mathematical formulation is carried out in a local cylindrical coordinate system $(\bar{r}, \theta, \bar{Z})$ in association with the local Cartesian coordinate system $(\bar{X}, \bar{Y}, \bar{Z})$ the origin of which is located at the crack tip lying in the plate middle plane. In view of the local coordinate system chosen, it is necessary to consider for analysis only the region defined by $-a \leqslant \bar{X} \leqslant (B-a)$, $-L \leqslant \bar{Y} \leqslant L$ and $-h \leqslant \bar{Z} \leqslant h$ with appropriate continuity conditions at $\bar{X} = -a$, where $2a$ is the crack length, and other boundary conditions of the problem (Fig. 2). In the local coordinate system, the relations $\bar{X} = \bar{r}\cos\theta$, $\bar{Y} = \bar{r}\sin\theta$ and $\bar{Z} = \bar{Z}$ between the Cartesian and cylindrical coordinate system are valid.

It is convenient to introduce the following nondimensionalization of the coordinate systems $(\bar{X}, \bar{Y}, \bar{Z})$ and $(\bar{r}, \theta, \bar{Z})$, and other related quantities:

$$\bar{r}/a = r, \quad \theta = \theta, \quad \bar{Z}/a = \zeta, \quad \bar{X}/a = X = r\cos\theta, \quad \bar{Y}/a = Y = r\sin\theta$$

$$a\bar{\alpha} = \alpha = \frac{\partial}{\partial r}, \quad a\bar{\beta} = \beta = \frac{1}{r}\frac{\partial}{\partial\theta}, \quad (\,)' = \frac{\partial}{\partial\zeta}, \quad \alpha^2 = \frac{\partial^2}{\partial r^2}$$

$$\beta^2 = \frac{1}{r}\alpha + \frac{1}{r^2}\frac{\partial^2}{\partial\theta^2}, \quad a^2D^2 = \delta^2 = \alpha^2 + \beta^2, \quad \eta = h/a, \quad \nabla^2 = \delta^2 + \frac{\partial^2}{\partial\zeta^2}$$

where

$$D^2 = \frac{\partial^2}{\partial \bar{x}^2} + \frac{\partial^2}{\partial \bar{y}^2}$$
$$= \frac{\partial^2}{\partial \bar{r}^2} + \frac{1}{\bar{r}}\frac{\partial}{\partial \bar{r}} + \frac{1}{\bar{r}^2}\frac{\partial^2}{\partial \theta^2}.$$

It may be noted that, with the above notation, the limit $-h \leqslant \bar{Z} \leqslant h$ corresponds to $-\eta \leqslant \zeta \leqslant \eta$. In later developments the following notation with respect to Poisson's ratio μ would be useful:

$$\mu_1 = 1/(1-\mu), \quad \mu_2 = 1/(1-2\mu), \quad \mu_3 = \mu/(1-2\mu).$$

Governing equations

The governing partial differential equations of the problem are the equations of equilibrium in terms of the displacement components $\bar{u}$, $\bar{v}$ and $\bar{w}$ along the $\bar{r}$-, θ- and $\bar{Z}$-directions, as derived from the three-dimensional equations of the theory of elasticity. The corresponding equations in the non-dimensionalized cylindrical coordinate system (r, θ, ζ) are given as[13, 14]

$$[\nabla^2 - 1/r^2]u - (2/r)\beta v + \mu_2 \alpha \rho = 0$$
$$[\nabla^2 - 1/r^2]v + (2/r)\beta u + \mu_2 \beta \rho = 0$$
$$\nabla^2 w + \mu_2 \rho' = 0 \tag{1}$$

where

$$\rho' = \frac{\partial \rho}{\partial \zeta}.$$

In eqns (1), u, v and w are the non-dimensionalized displacement components along the r-, θ- and ζ-directions, respectively, as defined by $u = \bar{u}/a$, $v = \bar{v}/a$, and $w = \bar{w}/a$. Also, in this equation, ρ is the dilatation given by

$$\rho = \alpha u + \beta v + \frac{u}{r} + w'. \tag{2}$$

The expressions for the stresses $(\sigma_r, \sigma_\theta, \sigma_z, \sigma_{r\theta}, \sigma_{rz}, \sigma_{\theta z})$ in terms of the displacement components, as derived from Hooke's law, are given as[13]

$$\sigma_r/2G = \alpha u + \mu_3 \rho$$
$$\sigma_\theta/2G = (\beta v + u/r) + \mu_3 \rho$$
$$\sigma_z/2G = w' + \mu_3 \rho$$
$$\sigma_{r\theta}/2G = \tfrac{1}{2}(\beta u + \alpha v - v/r)$$
$$\sigma_{rz}/2G = \tfrac{1}{2}(\alpha w + u')$$
$$\sigma_{\theta z}/2G = \tfrac{1}{2}(\beta w + v'). \tag{3}$$

Boundary conditions

Solution to the governing equations, eqns (1), must satisfy the boundary conditions of the problem, which include those at the plate faces, crack surfaces, and at the exterior edges of the plate (Fig. 2). They can be written as:

exterior edges of the plate

$$\text{at} \quad X = -1, \quad u_x = \sigma_{xz} = \sigma_{xy} = 0 \tag{4}$$

$$\text{at} \quad X = B/a - 1, \quad \sigma_x = \sigma_{xy} = \sigma_{xz} = 0 \tag{5}$$

$$\text{at} \quad Y = \pm L/a, \quad \sigma_y = (\sigma_b)\bar{Z}/h = (3M_0/2h^2)\bar{Z}/h, \quad \sigma_{yz} = \sigma_{xy} = 0 \tag{6}$$

where M_0 is the applied bending moment;

plate faces ($\bar{Z} = \pm h$ or $\zeta = \pm h/a = \eta$)

$$\sigma_{rz} = \sigma_{\theta z} = \sigma_z = 0; \tag{7}$$

crack surfaces ($\theta = \pm\pi$)

$$\sigma_{r\theta} = \sigma_\theta = \sigma_{\theta z} = 0. \tag{8}$$

In eqns (4)–(6), u_x is the displacement component along the X-direction while σ_x, σ_y, σ_{xy}, σ_{xz} and σ_{yz} are the stress components in the (X, Y, ζ) coordinate system. It is to be noted here, that eqns (4) actually represent the continuity conditions, referred to earlier (Fig. 1).

It is to be noted that in eqns (4)–(8), only X, Y, ζ and u_x are dimensionless. Further formulation will be developed in the non-dimensional (r, θ, ζ) system. However, the coordinate $\bar{Z}$, wherever it occurs, appears as $\bar{Z}/h$, in association with h.

Solution

Nature of the proposed solution. The total solution to the governing equations, eqns (1), which is proposed herein, consists of three independent solutions which, individually, satisfy eqns (1). The first independent solution which is herein referred to as the symbolic solution is constructed by following Lur'e's[13] symbolic method of constructing solutions to eqns (1). The second independent solution is called the "elementary" solution, while the third independent solution may be referred to as the "associated" solution. In arriving at these three solutions, the procedure introduced by Lur'e[13], in which the quantities α, β and δ are regarded as numbers, has been followed. The above three independent solutions, individually, satisfy the boundary condition at the plate faces as defined by eqns (7). The above three independent solutions are allowed to satisfy together the boundary conditions at the crack surfaces and, also, those at the exterior edges of the plate as defined by eqns (8) and (4)–(6).

The total solution to the governing equations, eqns (1), consisting of the above-mentioned three independent solutions may be written as

$$\begin{aligned} u &= -\eta\alpha(\psi_1\psi + \chi_1\chi) + \beta(s/\delta)\Omega \\ v &= -\eta\beta(\psi_1\psi + \chi_1\chi) - \alpha(s/\delta)\Omega \\ w &= \psi_2\psi + \chi_2\chi \end{aligned} \tag{9}$$

where ψ, χ and Ω, which correspond to "symbolic", "elementary" and "associated" solutions, respectively, are functions of the r- and θ-coordinates only, and are solutions of the following differential equations:

$$[\delta^2-(\omega_k/\eta)^2]\psi = 0$$
$$[\delta^2-(l'\pi/\eta)^2]\Omega = 0$$
$$\delta^4\chi = 0. \tag{10}$$

In eqns (9) and (10), $S = \sin \delta z$, and ω_k are the complex roots of the equation $\sin 2\omega_k - 2\omega_k = 0$, $k = 1, 2, 3, \ldots, \infty$. Here, $l' = l + 1/2$ with the range for l defined as: $l = 0, 1, 2, 3, \ldots, \infty$. The functions ψ_1, ψ_2, χ_1 and χ_2 of eqns (9), which are functions of the z-coordinate only, are given as

$$\psi_1(\zeta) = (1-2\mu)S\bar{C}/\delta\eta + (\zeta/\eta)C\bar{C} + S\bar{S}$$
$$\psi_2(\zeta) = 2(1-\mu)C\bar{C} + \delta\zeta S\bar{C} - \eta\delta\bar{S}C$$
$$\chi_1(\zeta) = 2(1-\mu)(1-\delta^2\eta^2)\zeta/\eta + (2-\mu)\delta^2\eta^2\{\zeta/\eta - 1/3(\zeta/\eta)^3\}$$
$$\chi_2(\zeta) = 2(1-\mu) - \delta^2\eta^2\{2(1-\mu) + \mu(1-\zeta^2/\eta^2)\} \tag{11}$$

where

$$C = \cos \delta\zeta.$$

In eqns (11), $\bar{S}$ and $\bar{C}$ are the values of S and C at the plate faces ($\zeta = \pm\eta$ or $Z = \pm h$). The solutions to the differential equations, eqns (10), may be taken in the following form:

$$\psi(r, \theta) = \mathrm{Re} \sum_n \sum_{k=1}^{r} d_{kn} I_n(\omega_k r/\eta) \cos n\theta$$
$$\chi(r, \theta) = \sum_n \sum_{m=0}^{t} r^l [M_l \cos (l-2)\theta + N_l \cos l\theta]$$
$$\Omega(r, \theta) = \sum_n \sum_{l=0}^{t} C_{ln} I_n(l'\pi r/\eta) \sin n\theta \tag{12}$$

where

$$l = n + 2m.$$

In eqns (12), I_n are modified Bessel functions of the first kind. Here, d_{kn} are unknown complex constants, while C_{ln}, M_l and N_l are real constants. The range of n appearing in these equations will be discussed later. It is to be noted from eqns (9)–(12) that the solutions u, v and w to the governing equations, eqns (1), satisfy the boundary conditions at the plate faces as given by eqns (7), and the unknown constants d_{kn}, C_{ln}, M_l and N_l are to be determined from the satisfaction of other boundary conditions of the problem, namely eqns (4)–(6) and (8). The expressions for the stress components can be determined by substituting eqns (9) into eqns (3).

An inspection of the three component solutions, namely the "symbolic", "elementary" and "associated" solutions (which are associated with the functions ψ, χ and Ω, respectively), reveals that the stress and displacement fields produced by any one of these three solutions are different from those of the other two. The presence of this feature establishes the independence of the three component solutions, which together form the total solution as defined by eqns (9).

Satisfaction of crack surface boundary conditions and range of n

In order to facilitate the satisfaction of the crack surface boundary conditions (8) (at $\theta = \pm\pi$), it is necessary to express the stresses involved in power series form in r and Fourier series form in ζ involving $C_l(\zeta)$ or $S_l(\zeta)$, as the case may be, where $C_l(\zeta) = \cos l'\pi\zeta/\eta$ and $S_l(\zeta) = \sin l'\pi\zeta/\eta$. It is to be noted that the stress components as determined from the

"associated" solution are obtained in a Fourier series form in the ζ-coordinate (as they appear in their original form). Therefore, it is only necessary to express the stress components associated with the "symbolic" and "elementary" solutions in Fourier series form. Noting that the original form of these solutions with respect to the ζ-coordinate involves such terms as $\overset{\bullet}{S}$, $\overset{\bullet}{C}\zeta$, $\overset{\bullet}{C}$, $\overset{\bullet}{S}\zeta$ (where $\overset{\bullet}{S} = \sin \omega_k \zeta, \eta$ and $\overset{\bullet}{C} = \cos \omega_k \zeta, \eta$), appropriate relations connecting these terms to $C_l(\zeta)$ or $S_l(\zeta)$, as the case may be, are used[15]. In dealing with the r-coordinate, the modified Bessel functions $I_n(\Gamma r/\eta)$ with $\Gamma = \omega$ or $l'\pi$, can be expressed in series form in powers of r by using the power series expansion of Bessel functions[16]. The Appendix gives σ_n expressed in this form. The expressions for other stress and displacement components can be obtained in similar forms. Having expressed the stresses involved ($\sigma_n, \sigma_m, \sigma_{nz}$) in appropriate forms, the boundary conditions at the crack surfaces ($\theta = \pm\pi$) may now be satisfied for each power of r and with respect to each value of l appearing in these series expansions.

At this point it is appropriate to consider the range of n in the series expansions occurring in the expressions for the stresses and displacements. In this connection it may be recalled that the order n of modified Bessel functions, I_n, consists both of fractional and integer values, and may include positive as well as negative values. Also the satisfaction of crack surface boundary conditions suggests that n should be expressed as follows: $n = 2j \pm 1/2$, $n = 2j$ and $n = 2j+1$, where j is assigned positive as well as negative values. The actual permissible range of n is governed by the condition that the displacement components (u, v, w) at the crack front are finite. Due to this requirement $n \geqslant (-1/2)$. The condition of finiteness of displacements at the crack front is enforced on the solution solely from physical considerations, and in ensuring this condition it is the total solution that must be considered (u, v, w as given by eqns (9)). When the condition of finiteness of all the three displacement components at the crack front is enforced on the total solution of the problem, two groups of ranges for n are found to be valid

$$\begin{aligned} &\text{Group 1}: n = 2j \pm 1/2, \quad j = 0, 1, 2, \ldots, \infty \\ &\text{Group 2}: n = 2j+1 \text{ and } 2j, \quad j = 0, 1, 2, \ldots, \infty. \end{aligned} \tag{13}$$

In assigning values to n some particular cases need special treatment. The rigid body displacements arising from terms such as a constant and $r\cos\theta$, which are obtained when $n+2m = 0$ and 1, have been retained. However, terms such as $\ln r$, also derived from $n+2m = 0$, have been excluded from the analysis, since they produce infinite displacements at the crack front.

In satisfying the boundary conditions at the crack surfaces, both fractional and integer values must be assigned to n, according to Groups 1 and 2 defined in eqns (13).

Satisfaction of crack surface boundary conditions as described above leads to four sets of homogeneous algebraic equations corresponding to Groups 1 and 2. Each equation involves the unknown constants N_l, M_l, d_{kn} and C_{ln}. The constants are determined from the satisfaction of the boundary conditions at the exterior of the plate, as given by eqns (4)–(6).

Boundary conditions at the exterior (outer) edges of the plate

Since the solution has been obtained in the cylindrical coordinate system (r, θ, ζ) and the exterior edges of the plate are rectilinear, these boundary conditions must be satisfied by the boundary point least squares method with respect to the (r, θ, ζ) coordinates, in association with the (X, Y, ζ) coordinates. In order to reduce the analytical and numerical work involved in satisfying these boundary conditions to manageable proportions, the stress boundary conditions of eqns (4)–(6) must be satisfied in terms of stress resultants and stress couples rather than unit stresses. The boundary condition $u_z = 0$ appearing in eqn (4) is replaced by its equivalent $\phi_z = 0$ where ϕ_z is the average rotation about the Y-axis at the edge $X = -1$. The corresponding modified boundary conditions may be written as

$$\text{at} \quad X = -1, \quad \phi_x = Q_x = M_{xy} = 0$$

$$\text{at} \quad X = B/a - 1, \quad M_x = M_{xy} = Q_x = 0$$

$$\text{at} \quad Y = \pm L/a, \quad M_y = M_0$$

the applied uniform moment

$$Q_y = M_{xy} = 0 \tag{14}$$

where

$$\phi_x = 12/(2h)^3 \int_{-h}^{h} u_x \bar{Z}\, \mathrm{d}\bar{Z}. \tag{15}$$

RESULTS AND DISCUSSION

Nature of stresses in power series form in r

The expressions for the stress components are obtained in series form in powers of r, e.g. expressions for σ_θ given in the Appendix. It may be observed from the expression for σ_θ that the values for n as determined from eqns (13), when substituted into the series expansions, lead to r terms containing both positive and negative powers. A consideration of only negative powers leads to such tems as $r^{-1/2}, r^{-1}, r^{-3/2}, r^{-5/2}, \ldots$, in decreasing order. When the condition of finiteness of displacement components at the crack front is enforced on the solution, it is found that all the r terms with negative powers vanish except for the $r^{-1/2}$ term. Thus, the only term which can lead to singular stresses is the $r^{-1/2}$ term. It may be mentioned here that the behaviour of other stress components, except for transverse shear stresses, is similar. The transverse shear stresses are of the order of unity.

Mathematical expression for the stress intensity factor

The state of stress in the neighbourhood of the crack front is of special interest in a crack problem. In this region, where $r \ll 1$, the stress distribution can be expressed as

$$\sigma_r = K_b(\bar{Z})[1/4(2\bar{r})^{1/2}](5\cos\theta/2 - \cos 3\theta/2) + O(1)$$

$$\sigma_\theta = K_b(\bar{Z})[1/4(2\bar{r})^{1/2}](3\cos\theta/2 + \cos 3\theta/2) + O(1)$$

$$\sigma_{r\theta} = K_b(\bar{Z})[1/4(2\bar{r})^{1/2}](\sin\theta/2 + \sin 3\theta/2) + O(1)$$

$$\sigma_z = \dot{K}_b(\bar{Z})[4\mu/2(2\bar{r})^{1/2}]\cos\theta/2 + O(1) \tag{16}$$

$$\sigma_{rz} = O(1), \quad \sigma_{\theta z} = O(1). \tag{17}$$

It may be observed from eqns (16) and (17) that the in-plane stresses σ_r, σ_θ and $\sigma_{r\theta}$ as well as the transverse normal stress σ_z are singular with an inverse square root singularity $(1/r^{1/2})$, while the transverse shear stresses σ_{rz} and $\sigma_{\theta z}$ are of the order of unity. In these equations $K_b(\bar{Z})$ is the stress intensity factor and $\dot{K}_b(\bar{Z})$ the factor associated with the singular term of σ_z. The expressions for these factors are given as

$$K_b(\bar{Z}) = (2a)^{1/2}(4G)\sum_{l=0}^{\infty}(-1)^{l+1}S_l(\bar{Z})[4M_{3/2}(1+\mu)/(l'\pi)^2 + \mathrm{Re}\sum_{k=1}^{\infty} d^*_{k(-1/2)}(\omega_k^2/\eta^2)\{\mu a_{kl} - (1+\mu)g_{kl}\}] \tag{18}$$

$$\dot{K}_b(\bar{Z}) = (2a)^{1/2}(4G)\sum_{l=0}^{\infty}\mathrm{Re}\sum_{k=1}^{\infty}(-1)^{l+1}S_l(\bar{Z})d^*_{k(-1/2)}(\omega_k^2/\eta^2)a_{kl}/\mu \tag{19}$$

where

$$S_l(\bar{Z}) = \sin l'\pi\bar{Z}/h = \sin l'\pi\zeta/\eta.$$

In eqns (18) and (19), $d^*_{n(-1/2)}$ and $M_{3/2}$ are the constants, referred to earlier, with respect to $n = -1/2$.

At this point it is useful to study whether the expression for the SIF as given by eqn (18) would permit any manipulation. Such a process may throw some light on the characteristics of various terms involved in this equation. In this connection, it may be observed that the first term in eqn (18) for K_b, associated with the constant $M_{3/2}$, can be reduced to a simpler form. Denoting the first term by $K_b^{(1)}$ and the second term associated with the constant $d^*_{n(-1/2)}$ by $K_b^{(2)}$, it is noted that $K_b = K_b^{(1)} + K_b^{(2)}$. The simpler form of the first term can now be expressed as

$$K_b^{(1)}/\sigma_b a^{1/2} = -\sqrt{2}(1+\mu)(\bar{D}/M_0)B_{3/2}(\bar{Z}/h) \tag{20}$$

where

$$B_{3/2} = 2(1-\mu)M_{3/2}/a. \tag{21}$$

In deriving expression (20) the following relations have been used:

$$\bar{Z}/h = 2\sum_{l=0}^{r}(-1)^l S_l(\bar{Z})/(l'\pi)^2$$

$$\bar{D} = (2/3)[Eh^3/(1-\mu^2)]$$

$$M_0 \text{ (applied moment loading)} = (2/3)\sigma_b h^2.$$

The expression for $K_b^{(1)}$, as given by eqn (20), has now assumed a simpler form and involves a variation in Z which is linear in form. It is interesting that at the plate faces ($\bar{Z} = \pm h$), eqn (20) becomes identical to eqn (2.39) of Ref. [17] where Reissner's theory has been used, provided $B_{3/2}$ of eqn (21) is set equal to $A_{3/2}/\sqrt{a}$. In making this comparison, care has been taken to verify that $B_{3/2}$ possesses the same dimension as that of $A_{3/2}/\sqrt{a}$ in Ref. [17].

Thus, it is seen that the first term of the expression for SIF, as defined by eqn (18), represents the SIF of the corresponding two-dimensional bending problem of Reissner's theory. It is, therefore, evident that the second term on eqn (18), which does not permit any simplification of its form, imparts the required three-dimensional character to the expression for the stress intensity factor. It is interesting to note that the expression for $\overset{*}{K}_b$, representing the singular transverse normal stress, does not permit any simplification in its form analogous to that of the first term of eqn (18). This behaviour is to be expected since Reissner's two-dimensional formulation involves the disappearance of the transverse normal stress everywhere.

Some important features exhibited by the stress state and displacement field in the neighbourhood of the crack front

It may be observed from eqns (16) that the in-plane stresses ($\sigma_r, \sigma_\theta, \sigma_{r\theta}$) and the transverse normal stress σ_z in the neighbourhood of the crack front, contain inverse square root singularity. The transverse shear stresses are of the order of unity, as can be observed from eqns (17). The angular variation of the singular stresses is the same as that of the two-dimensional plane strain problem. The stress intensity factor is found to depend on $\bar{Z}$ and the thickness parameter $\eta(=h/a)$, the actual variation with respect to $\bar{Z}$ is in the form of a Fourier series. A mathematical study of the expression for the SIF as given by eqn (18) indicates that $K_b(\bar{Z})$ does not vanish at the plate faces $\zeta = \pm\eta$ (or $\bar{Z} = \pm h$). It is to be noted that $K_b(\bar{Z})$ vanishes at the plate faces, thereby leading to the disappearance of the singular part of σ_z there. This behaviour is to be expected since the condition $\sigma_z = 0$ formed one of the boundary conditions at the plate faces (eqn (7)). It is noteworthy that all the

displacement components are finite at the crack front; this condition was, in fact, enforced on the total solution of the problem solely from physical considerations. It is to be noted that the above-mentioned features concerning the type of stress singularity, and angular variation of singular stresses were also observed in the corresponding three-dimensional analysis of the extension problem[6].

A comparison study of the present results with the existing two-dimensional results from Reissner's theory[17–19] indicate that the type of stress singularity, nature of the angular variation of singular stresses and character of transverse shear stresses around the crack front are the same. In contrast, the results from classical theory exhibit the following features: (i) the angular variation of singular stresses is dependent on Poisson's ratio, (ii) the transverse shear stresses are singular with a singularity of $1/r^{3/2}$[20, 21], and (iii) the in-plane stresses exhibit the inverse square root singularity. It may be observed that only the last feature is in agreement with the present results.

The stress intensity factor $K_b(\bar{Z})$ of the present bending problem is found to be a function of the $\bar{Z}$-coordinate and the thickness ratio $\eta(=h/a)$. In this connection various aspects of the SIF have been discussed by Sih[22], in particular at the corner points where the crack penetrates the faces of the plate. Sih and co-workers[1, 22] have pointed to the disappearance of SIF at the plate faces as an unsound feature, intuitively. The SIF as defined by $K_b(\bar{Z})$ in eqn (18) does not vanish at the plate faces. In discussing the nature of SIF variation across the thickness, it may be mentioned that the formulations based on the classical theory and Reissner's theory lead to stress intensity factors with only a linear variation across the thickness. However, the improved bending theory proposed by Hartranft and Sih[8] and Sih[23] leads to the SIF with a general variation across the plate thickness. This result occurs even though the theory proposed is two-dimensional in character for plates with a through-crack geometry and stress-free plate faces.

It may be observed from expression (19) for $\overset{*}{K}_b(\bar{Z})$, the factor associated with the singular term of σ_z, that this quantity is a function of the Z-coordinate in the form of a Fourier series. The important feature of this stress (σ_z) lies in its general variation across the thickness, in the zone lying between the plate faces and the plate middle plane. In contrast, the transverse normal stress σ_z vanishes, completely, everywhere in the plate domain in the analysis of crack problems where the formulation is based on Reissner's theory. This is also true of the higher order theories proposed by Sih[23], and Hartranft and Sih[8] in situations where the plate faces ($\bar{Z} = \pm h$) experience stress-free conditions. The significant feature to be noted here is that even the higher order plate bending theories proposed by these authors, where all the six components of the stress field have a general variation with respect to the Z-coordinate (across the thickness), reduce to one with all the characteristics of two-dimensional sixth-order (Reissner's) plate theory. This is by virtue of the transverse normal stress vanishing everywhere in the plate domain. It is noteworthy that in the present analysis σ_z and $\partial\sigma_z/\partial\zeta$ vanish at the plate faces, as can be observed from the expression for $\overset{*}{K}_b(\bar{Z})$. This feature arises from the disappearance of the transverse shear stresses and a consideration of the equations of equilibrium along the Z-direction, at the plate faces.

Finally, it is noteworthy that all the displacement components are finite along the crack front. In fact, this condition was enforced on the solution solely from physical considerations. This same procedure was followed by other investigators[1, 2].

In the preceding discussion some of the important features of the results obtained in the neighbourhood of the crack front were brought out solely from the mathematical form of eqns (16)–(19). Their significance was discussed in the light of the existing results from two-dimensional investigations. It will be interesting to determine the nature of the results for this region that may emerge following numerical studies.

Discussion of numerical results—a comparison study with existing results

Three-dimensional finite element results presented by Hilton and Sih[9], and Alwar and Nambissan[10] can be used for comparison purposes. The variation of SIF across the

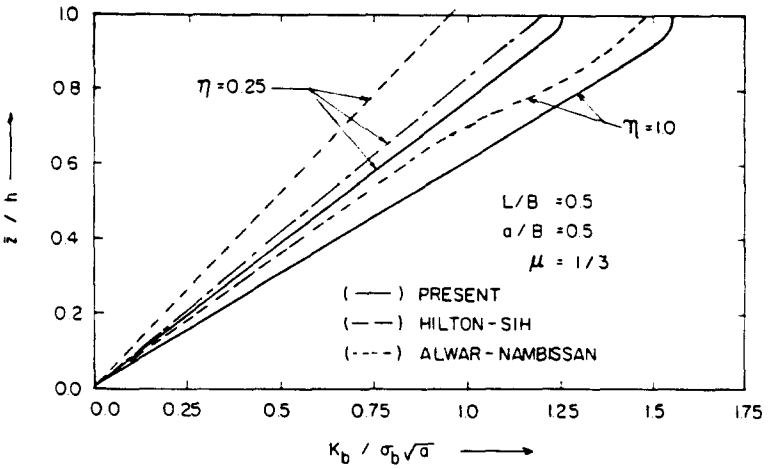

Fig. 3. Comparison of present results for SIF (variation across thickness) with FEM results.

thickness obtained by the present method for the plate geometry $L/B = 0.5$ and $a/B = 0.5$ corresponding to two thickness ratios, namely $\eta = 0.25$ and 1.0 are shown in Fig. 3. Here, μ was taken to be equal to 1/3. Also shown in this figure are the corresponding distributions for $\eta = 0.25$ obtained by Hilton and Sih[9] and by Alwar and Nambissan[10]. For $\eta = 1.0$ the results of Alwar and Nambissan are provided. It may be observed from this figure that for the case with $\eta = 0.25$, the present method furnishes results for the SIF variation which is almost linear for the major part of the thickness except in the vicinity of the plate faces. The corresponding FEM results indicate a linear variation all through the thickness of the plate. In addition, for this thickness ratio ($\eta = 0.25$), while the results of Hilton and Sih are in good agreement with the present values (within 4% at the plate faces) those of Alwar and Nambissan are observed to deviate from the present results significantly (24.8% at the plate faces). For the case with $\eta = 1.0$, the results of the present method are in reasonable agreement with FEM results at the plate faces (within 5.2%). However, the SIF variations across the thickness are themselves not in good agreement for the plate region lying outside the mid-thickness region. It is interesting to note that at the plate faces, the percentage difference between the present results and those of Alwar and Nambissan tends to decrease gradually as the thickness ratios increase from $\eta = 0.25$ to 1.0. From Fig. 4 for the plate geometry $L/B = 0.5$, $a/B = 1/3$ and $\eta = 1.125$, the present results for the SIF are in close agreement with those of Alwar and Nambissan except in a small region near the plate faces, where the differences experienced between the two results are less than 4%. It is significant that the thickness ratio of 1.125, associated with a percentage difference of 4 as in Fig. 4, turns out to be larger than the η value of 1.0 associated with a percentage difference of 5.2

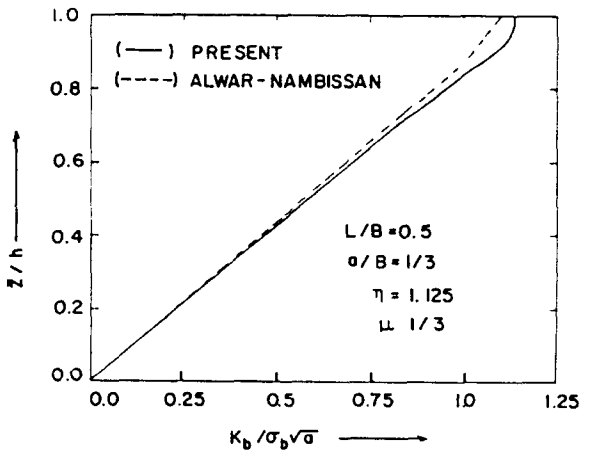

Fig. 4. Comparison of present results with FEM results for SIF variation across thickness.

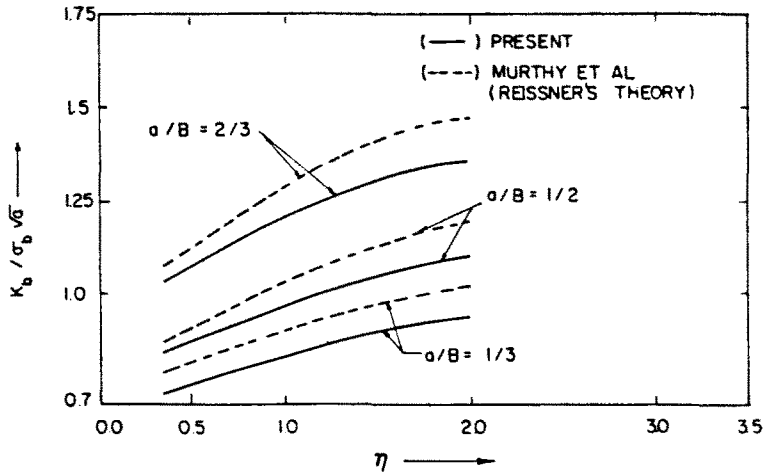

Fig. 5. Comparison of present results for SIF (at plate faces) with results from Reissner's theory for square plates ($L/B = 1.0$, $\mu = 1/3$).

as observed from Fig. 3. This suggests that the FEM results[10] are found to be in increasingly better agreement with the present results, as η values increase.

It appears that no new results from three-dimensional investigations, other than those of Hartranft and Sih[8] and Alwar and Nambissan[10] obtained by FEM, are available in the literature for the bending problem. In view of this, further comparison studies would be carried out with results from two-dimensional investigations. This would permit determination of three-dimensional effects and also an assessment of the order of accuracy of two-dimensional results.

The two-dimensional results from Reissner's theory obtained by Murthy *et al.*[18] have been used for comparison with the present three-dimensional values. The percentage differences between the three- and two-dimensional results have been plotted in Fig. 5. It may be observed from these results that, for a given value of the a/B ratio, as η increases the SIF values are also found to increase. However, the magnitude of these increases for the three-dimensional case is smaller than that for the two-dimensional case. In addition, as the a/B ratio increases, say from 1/3 to 2/3, the rate of increase of SIF values with η is also observed to increase. It may be mentioned here that the percentage differences between the three- and two-dimensional results are found to increase with increases in η values, for a given value of the a/B ratio. It is interesting to note that the percentage differences associated with various η values for the case with $a/B = 1/3$ are larger than the corresponding values associated with either $a/B = 1/2$ or 2/3. Thus, Fig. 5 reveals that the three-dimensional effects on the state of stress are reflected by decreases in SIF values from their two-dimensional values, the magnitude of these decreases increasing with increases in the thickness ratio η, for all cases of width ratios (a/B) considered.

Another interesting aspect of the results to be considered is the variation of SIF through the thickness of the plate. Figure 6 shows a comparison of the SIF variations across the thickness as determined by the present method with those obtained from Reissner's theory by Murthy *et al.*[18] for three different thickness ratios, namely $\eta = 0.35$, 1.0 and 2.0. It can be observed from this figure that for the three-dimensional case the SIF variation in the mid-thickness region (say up to about $\bar{Z} = 0.6h$) is linear, for all three η values considered. However, beyond the mid-thickness region, the SIF varies in a non-linear manner, the intensity of nonlinearity increasing with increases in η values. In contrast, the corresponding distributions for SIF for the two-dimensional case as determined from Reissner's theory are completely linear all through the plate thickness. This behaviour is to be expected since the stress intensity factor is, mathematically, found to have a $\bar{Z}$-dependency which is linear in form. It is significant that the most interesting aspect of the SIF variation across the thickness occurs at the free surfaces of the plate, $\bar{Z} = \pm h$. It assumes maximum values there for both three- and two-dimensional cases, as can be observed from Fig. 6.

It has been noted earlier that not only the in-plane stresses but also the transverse normal stress are singular. It is appropriate now to consider the case of the singular

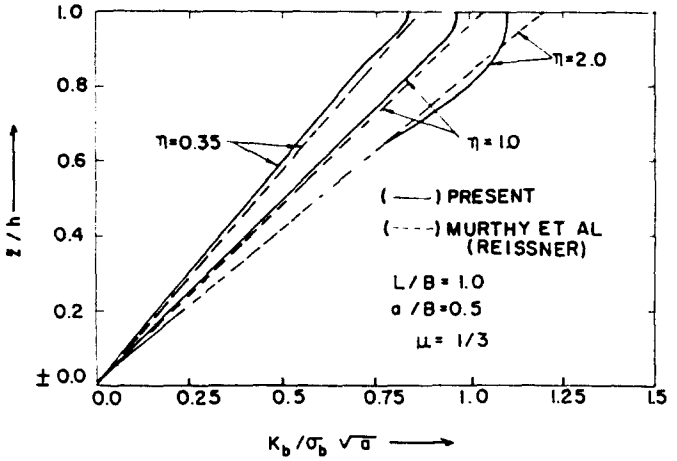

Fig. 6. Comparison of present results for SIF (variation across thickness) with Reissner's results.

transverse normal stress. In this connection, it may be stated that, since the transverse normal stress σ_z vanishes everywhere in the plate domain in Reissner's formulation, no comparison study can be carried out. However, for completeness, a brief discussion on the character of the singular transverse normal stress from the present three-dimensional formulation seems to be appropriate. A plot of the variation of $\dot{K}_b(\bar{Z})$, which is the factor associated with the singular part of the transverse normal stress, is shown in Fig. 7. It may be noted from this figure that σ_z vanishes both at the plate middle plane and at the plate faces ($\bar{Z} = 0$ and $\pm h$). The vanishing character of this stress at the plate faces arises from the satisfaction of the boundary condition $\sigma_z = 0$, and the vanishing feature of this stress at the plate middle plane may be attributed to the antisymmetric nature of σ_z with respect to this plane. It is significant that, at the plate faces, not only the transverse normal stress but also its derivative with respect to the ζ-coordinate vanish. The disappearance of $\partial\sigma_z/\partial\zeta$ arises from the disappearance of the transverse shear stresses and a consideration of equilibrium in the Z-direction, at the plate faces.

At this point, it is useful to discuss the experimental results obtained by Mullinex and Smith[11] as well as Rubayi and Ved[12]. The results of Mullinex and Smith obtained from photoelastic studies indicate that the SIF, essentially, varies linearly across the thickness for a wide range of thickness ratios considered in the analysis. In contrast, the results of Rubayi and Ved, also from photoelastic studies, suggest a non-linear variation of stresses across the thickness, the nonlinearity increasing with increases in thickness ratios. While the results of Mullinex and Smith are in agreement with the theoretical prediction of Sih[23] for the thickness values lying in the thin plate range, the results of Rubayi and Ved are in

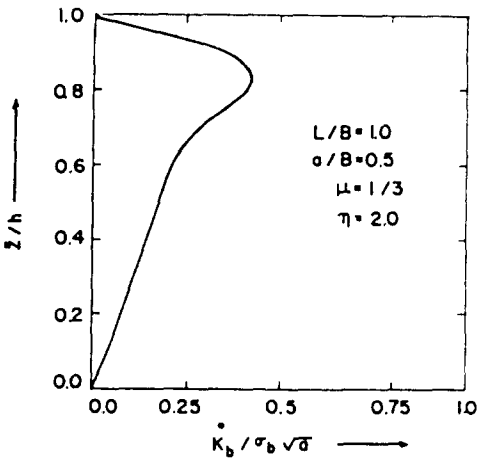

Fig. 7. Variation of transverse normal stress across thickness ($r \to 0$).

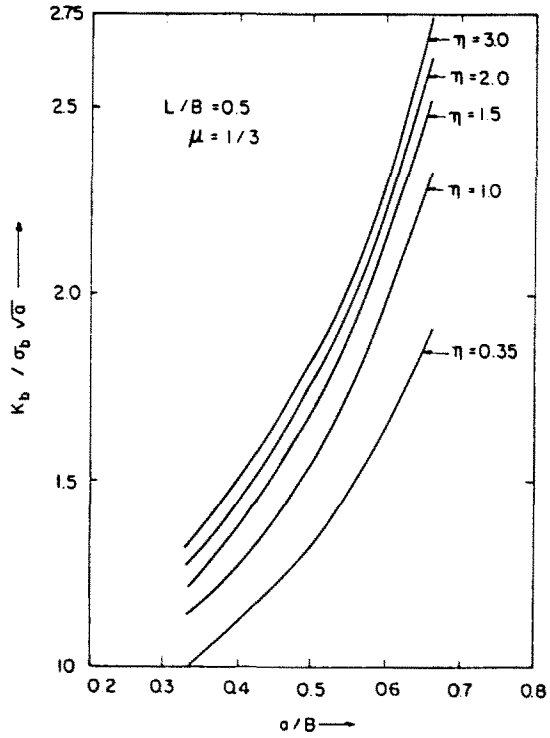

Fig. 8. Effect of width ratio on SIF values at plate faces ($\bar{Z} = \pm h$).

good agreement with those of Sih for all thickness ratios considered. In view of the widely varying nature of results presented in the above two photoelastic investigations a definite conclusion does not appear to be feasible, as far as the experimental results are concerned. On the other hand the results of Sih[23] (which are two-dimensional in nature for plates with stress-free faces, at $\bar{Z} = \pm h$, for reasons stated earlier), exhibit a stress state around the crack front the variation of which is nonlinear across the thickness, the extent of nonlinearity increasing with increases in the thickness ratios. Although a direct comparison of the present three-dimensional results with those of Sih[23] is not feasible in view of the differences in the plate geometry, these two results serve, at least, to suggest the presence of in-plane singular stresses. This indicates a non-linear variation for the SIF, with the intensity of nonlinearity increasing with increases in η values.

Effect of physical parameters on the stress intensity factor

The parameters influencing the behaviour of the stress intensity factor are the length ratio L/B, the width ratio a/B, the thickness ratio $\eta(=h/a)$ and Poisson's ratio μ. The effect of these parameters on the SIF has been studied in the numerical analysis. A discussion on various aspects in this regard are presented below.

Effect of a/B and L/B ratios. Figure 8 shows the variation of SIF at the plate faces ($\bar{Z} = \pm h$) with the a/B ratios for the case with $L/B = 0.5$ and $\mu = 1/3$ for various η values. It may be observed that for a given η value as the a/B ratio increases the SIF is also found to increase. But, for increasing η values, the rate of increase of SIF with the a/B ratio also correspondingly increases, particularly for large a/B values (the magnitude of the SIF value itself increases; this aspect will be considered later).

The influence of varying the length ratio L/B on the SIF values at the plate faces is shown in Fig. 9 for the case with $a/B = 0.5$ and $\mu = 1/3$, for various η values. It may be observed from this figure that as the length ratio increases the SIF decreases. It is interesting to note that the rate of decrease in the SIF values with the L/B ratio is found to be greater for small η values. In particular, it is observed that rapid decreases in SIF values occur in the region between $L/B = 0.5$ and 0.75. Thereafter, the curves tend to become flatter.

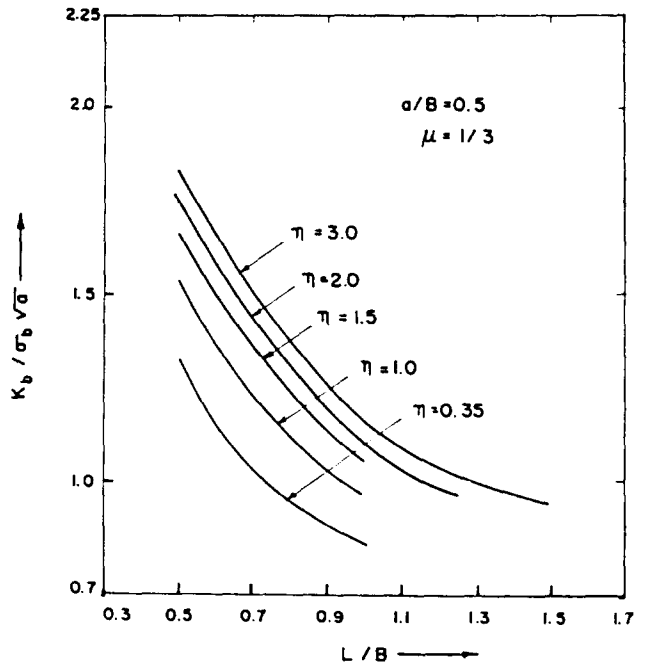

Fig. 9. Effect of length ratio on SIF values at plate faces ($\bar{Z} = \pm h$).

Effect of thickness ratio, η, and Poisson's ratio, μ. Among all the parameters, it appears, the influence of the thickness parameter η is the most important one. The influence of η on the stress intensity factor is observed in two different ways: its effect on the nature of SIF variation across the thickness, and its effect on the maximum SIF values. Figure 10 displays the nature of the changes produced on the SIF variation across the plate thickness by progressively increasing the η values from 0.25 to 3.0, the plate geometry considered is the case with $L/B = 0.5$, $a/B = 0.5$, and $\mu = 1/3$. In general, it is observed from this figure that in the region interior to the plate thickness the variation is linear for all the thickness ratios considered. Beyond the plate interior, as $\bar{Z}/h$ increases the variations tend to become nonlinear, the extent of nonlinearity increasing with increases in η values. In particular, it is noted that the most interesting aspect of SIF variations across the thickness occurs at the plate faces ($\bar{Z} = \pm h$), where the SIF reaches maximum values for all η values considered. An interesting plot of these maximum values as a function of the thickness ratio η is given in Fig. 11 (see the distribution corresponding to the case with $L/B = a/B = 0.5$). As can be observed, the maximum SIF values (at the plate faces) increase in magnitude with increases in the thickness ratio η. Again, an inspection of Fig. 10 reveals that in the region lying

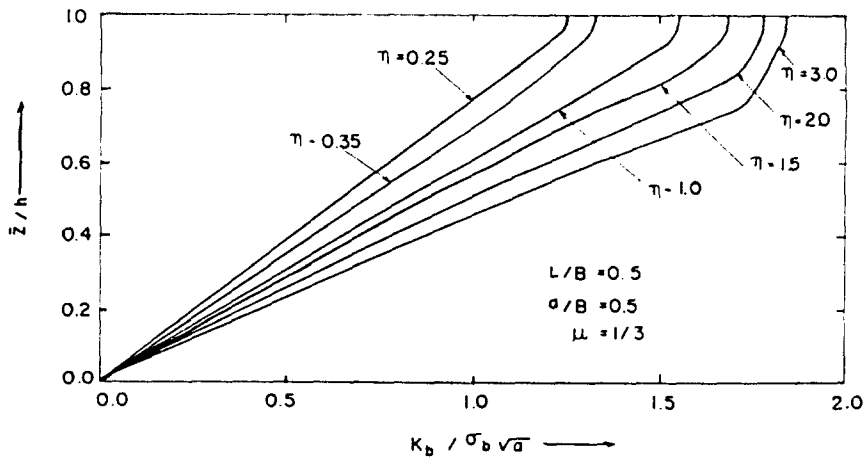

Fig. 10. Effect of thickness ratio on SIF variation across the thickness.

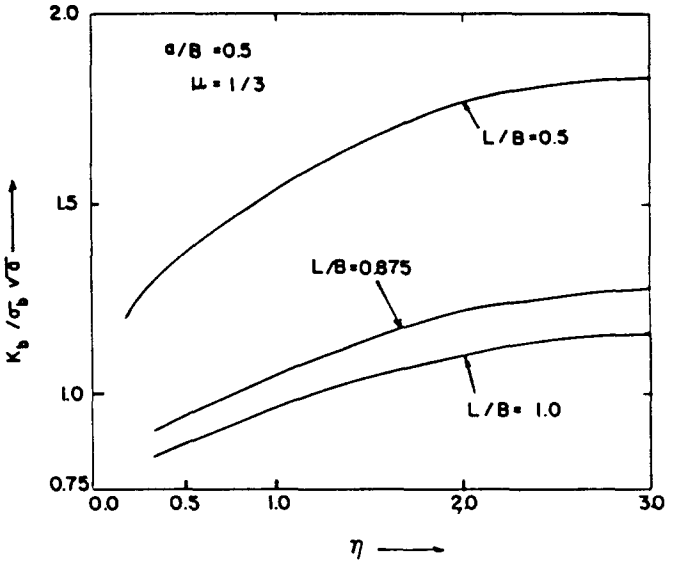

Fig. 11. Variation of maximum SIF values (at plate faces, $Z = \pm h$) with thickness ratio.

adjacent to the plate faces the SIF (e.g. see the distribution corresponding to $\eta = 3.0$) is found to decrease in magnitude with increases in the distance from the plate faces, but the rate of decrease brought about is, significantly, very small. However, after a certain distance is reached, this curve changes its course and approaches the region of linear variation. The region lying adjacent to the plate faces (or stress-free plate boundaries) can be conveniently referred to as the boundary layer region. In this new terminology, it may be stated that the boundary layer thickness (BLT) decreases with decreases in η values, as can be observed from Fig. 10. In other words, the BLT is found to increase as η increases. This behaviour, it appears, can be attributed to the vanishing of the transverse normal stress at the plate faces.

At this point, an intensive discussion on the character of SIF as observed in the boundary layer region is appropriate. In doing so, an analogy with the corresponding character of SIF observed in the extension problem[6] may lead to some interesting observations. In the extension problem, it was observed that as η was increased the BLT was found to decrease and the SIF experienced rapid drops in this region. In contrast, in the present bending problem, it is noted that with increases in η values the BLT is found to increase and, in addition, the SIF is also observed to increase. In fact, even a slightest hint of any decrease in SIF values is not observed across the plate thickness. Figure 11 shows the variation of SIF at the plate faces with η values for different L/B ratios. This figure indicates that the rate of increase of SIF values with η values increases with decreases in L/B values.

The effect of Poisson's ratio μ on SIF values is considered next. The effect of μ is to bring about a change in SIF variation across the thickness as well as at the plate faces. Figure 12 shows the nature of the changes brought about on the variation of SIF across the thickness for three different values of Poisson's ratio, namely 1/3, 0.4 and 0.45. The plate geometry considered here corresponds to $L/B = a/B = 0.5$, and $\eta = 3.0$. As can be observed from this figure, as μ increases, the SIF values are also found to increase all through the plate thickness. However, the extent of increases produced on SIF is largest in the boundary layer region. It is significant that the location of the maximum SIF value is not affected by increasing the μ values, in other words, the maximum SIF values are experienced at the plate faces only. In Fig. 13 the variation of maximum SIF values (at the plate faces) with the thickness ratio as influenced by increases in μ values is shown. It is clear from this figure that for a given value of η, the SIF value increases when μ is allowed to increase, from 1/3 (through 0.4) to 0.45. This phenomenon as observed in Fig. 13 was also noticed in the investigation carried out by Sih[23]. However, this comparison must be

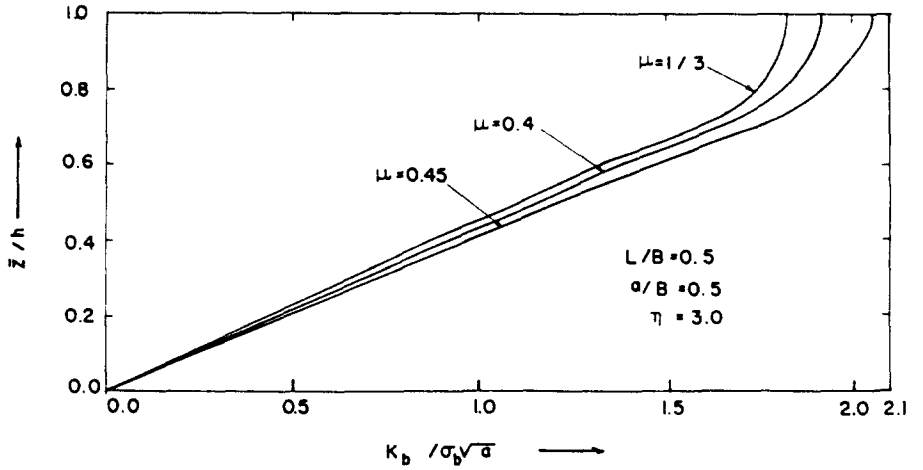

Fig. 12. Effect of Poisson's ratio on SIF variation across thickness.

viewed in a qualitative sense because of the differences in plate geometries considered in these two investigations.

Transverse normal stress, σ_z

At this point it is appropriate to study the behaviour of transverse normal stress, σ_z, for different η values. Figure 14 displays the variation of the singular part of the transverse normal stress across the thickness, for the case with $L/B = a/B = 0.5$ and $\mu = 1/3$ and for various values of the thickness ratio, η. Since $\dot{K}_b(\bar{Z})$ is the factor associated with the singular part of this stress, the variation of $\dot{K}_b$ (normalized with respect to $\sigma\sqrt{a}$) is shown in this figure. As mentioned earlier, the transverse normal stress is a function of the coordinate in the thickness direction $\bar{Z}$. It varies in an antisymmetric manner with respect to the plate middle plane and, also, vanishes at the plate faces ($\bar{Z} = \pm h$). It may be recalled that the disappearance of this stress together with the transverse shear stresses have formed boundary conditions (7). Besides, the disappearance of the transverse shear stresses and a consideration of the equilibrium condition along the $\bar{Z}$-direction at the plate faces imply the disappearance of the quantity $\partial\sigma_z/\partial\zeta$ at this boundary. The two features associated with the disappearance of σ_z and $\partial\sigma_z/\partial\zeta$ at the plate faces can be observed in Fig. 14. It may also be observed from this figure that the transverse normal stress, for any given value of η, reaches a maximum value at a particular point across the thickness and, thereafter, drops

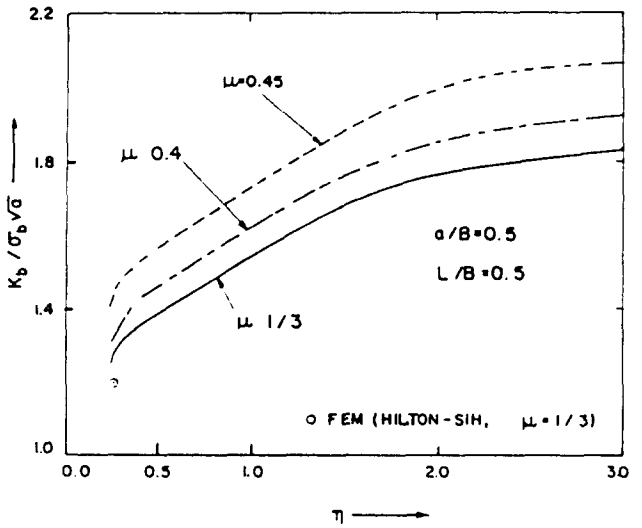

Fig. 13. Effect of η on SIF (at plate faces, $\bar{Z}/h = \pm 1$) for different μ values.

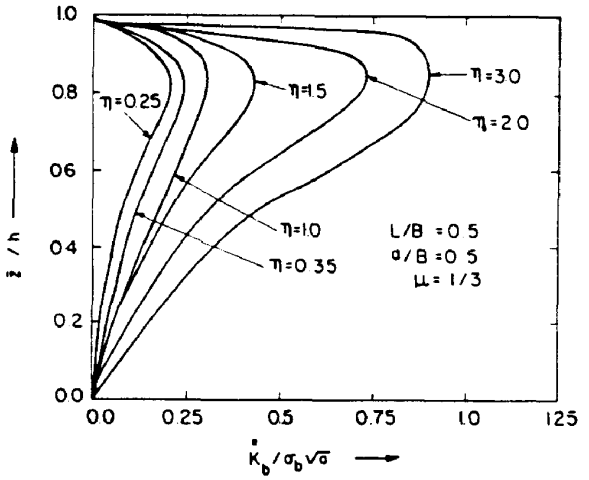

Fig. 14. Effect of thickness ratio on variation of σ_z in neighbourhood of crack front ($r \to 0$).

rapidly before finally vanishing at the plate faces. In particular, it may be seen that as η increases the maximum value of the stress is also found to increase. The locations where these maximum values occur are found to approach the plate faces as the thickness ratio η increases. It is believed that it is this phenomenon of increasing maximum stress values corresponding to increases in η values that has led to increases in the extent of the boundary layer region (as η increases), referred to earlier, in connection with the discussion of Fig. 10.

The results for σ_z of this paper will now be discussed in the light of previous work in this area. The results of other investigations concerning the nature of the transverse normal stress also will be briefly mentioned. In the photoelastic investigations of Rubayi and Ved[12] the results for this stress have not been presented. The photoelastic results of Mullinex and Smith[11] for the stress σ_z indicate that the variations of this stress across the thickness are similar to the corresponding variations of the present method only in a qualitative way (a direct comparison is not meaningful in view of vast differences in the plate geometries considered in the two investigations). In Refs [9, 10], finite element results for the transverse normal stress have not been presented. In discussing the transverse normal stress, it must be pointed out that the formulations based on Reissner's theory[18] and Sih's improved theories[23] lead to the disappearance of transverse normal stress everywhere in the plate domain, for cases with stress-free plate faces.

CONCLUSIONS

A general three-dimensional solution has been presented for the bending problem of finite thick plates with through-the-thickness cracks. It has been noted that the in-plane stresses and the transverse normal stress at the crack front are singular with an inverse square singularity, while the transverse shear stresses are of the order of unity. Among various parameters of the problem it is the thickness ratio which influences the SIF in a most significant manner. One of the important features of the solution lies in the character of the SIF variation across the thickness. Apart from being nonlinear, the SIF does not decrease as it varies across the thickness. This rules out the possibility of it disappearing at the plate faces as suggested in Ref. [9] and the maximum SIF value is thus achieved at the plate faces. In contrast to Reissner's theory which indicates a linear variation for the SIF, the results of this analysis show that the SIF variation across the thickness has a non-linear character. While in Reissner's theory the transverse normal stress vanishes everywhere in the plate domain, in the present analysis this stress has non-zero values.

REFERENCES

1. G. C. Sih, M. L. Williams and J. L. Swedlow, Three dimensional stress distribution near a sharp crack in a plate of finite thickness. AFML, Wright-Patterson Air Force Base, AFML-TR-66-242 (1966).

2. R. J. Hartranft and G. C. Sih, The use of eigenfunction expansions in the general solution of the three dimensional crack problems. *J. Math. Mech.* **19**, 123–138 (1969).
3. E. S. Folias, On the three dimensional theory of cracked plates. *J. Appl. Mech. ASME* **42**, 663–674 (1975).
4. E. S. Folias, Method of solution of a class of three dimensional elastostatic problems under Mode-I loading. *Int. J. Fracture* **16**, 335–348 (1980).
5. G. Villarreal, G. C. Sih and R. J. Hartranft, Photoelastic investigation of a thick plate with a transverse crack. *J. Appl. Mech. ASME* **42**, 9–14 (1975).
6. M. N. Bapu Rao, Three dimensional stress problem of a finite thick plate with a through-crack under tension. *Proc. Int. Conf. Frac.* (ICF6), New Delhi, Vol. 2, pp. 963–970 (1984).
7. I. S. Raju and J. C. Newman, Jr., Three dimensional finite element analysis of finite thickness fracture specimens. NASA-TND-8414.
8. R. J. Hartranft and G. C. Sih, Improved theories of the bending and extension of flat plates. In *Mechanics of Fracture—3, Plates and Shells with Cracks* (Edited by G. C. Sih), pp. 45–83. Noordhoff, Leyden, The Netherlands (1977).
9. P. D. Hilton and G. C. Sih, A specialized finite element approach for three dimensional crack problems. In *Mechanics of Fracture—3, Plates and Shells with Cracks* (Edited by G. C. Sih). Noordhoff, Leyden, The Netherlands (1977).
10. R. S. Alwar and K. N. Ramachandran Nambissan, Three dimensional finite element analysis of cracked thick plates in bending. *Int. J. Numer. Meth. Engng* **19**, 293–303 (1983).
11. B. R. Mullinex and C. W. Smith, Distribution of local stresses across the thickness of cracked plates under bending fields. *Int. J. Fracture* **10**, 337–352 (1974).
12. N. A. Rubayi and R. Ved, Photoelastic analysis of a thick square plate containing a central crack and loading by pure bending. *Int. J. Fracture* **12**, 435–451 (1976).
13. A. I. Lur'e, *Three Dimensional Problems of the Theory of Elasticity*. Interscience, New York (1964).
14. S. P. Timoshenko and J. N. Goodier, *Theory of Elasticity*, 3rd Edn. McGraw-Hill, New York (1970).
15. A. E. Green, The elastic equilibrium of isotropic plates and cylinders. *Proc. R. Soc.* **A195**, 533 (1949).
16. N. W. Maclachlan, *Bessel Functions for Engineers*. Clarendon Press, Oxford (1955).
17. S. Viswanath, On the bending of plates with through cracks from higher order plate theories. Thesis submitted to Indian Institute of Science, Bangalore, India (1985).
18. M. V. V. Murthy, K. N. Raju and S. Viswanath, On the bending stress distribution at the tip of a stationary crack from Reissner's theory. *Int. J. Fracture* **17**, 537–552 (1981).
19. R. J. Hartranft and G. C. Sih, Effect of plate thickness on the bending stress distribution around through cracks. *J. Math. Phys.* **47**, 276–291 (1968).
20. M. L. Williams, The bending stress distribution at the base of a stationary crack. *J. Appl. Mech.* **28**, 78–82 (1961).
21. G. C. Sih, P. C. Paris and F. Erdogan, Crack tip stress intensity factors for plane extension and plate bending problems. *J. Appl. Mech.* **29**, 306–312 (1962).
22. G. C. Sih, A review of the three dimensional stress problem for a cracked plate. *Int. J. Fracture Mech.* **7**, 39–61 (1971).
23. G. C. Sih, Bending of a cracked plate with an arbitrary stress distribution across the thickness. *J. Engng Ind.* **92**, 350–356 (1970).

APPENDIX

The expression for σ_{ii} in series form in powers of r is given as

$$\sigma_{ii} = \sum_{n} \sum_{l=0}^{4} 8G\eta(-1)^{l+1} S_l(z) \left[\sum_{m=0}^{4} q_l \{ t(1-t) N_t r^{t-2} \cos t\theta + [4/(1-\mu) - t](t-1) M_t r^{t-2} \cos (t-2)\theta + 4(\xi_l/q_l)\eta^2 (1-t)(t-2)(t-3) M_t r^{t-4} \cos (t-2)\theta \}_l + \{(-1)^l/(4l'\pi)\alpha\beta\Omega_{in}(r,\theta)\}_l \right]$$

where

$$\psi_{kn} = d_{kn} I_n(\omega_k r/\eta) \cos n\theta$$
$$\Omega_{in} = C_{in} I_n(l'\pi r/\eta) \sin n\theta$$
$$g_{kl} = (l'\pi)^2/[\omega_k^2 - (l'\pi)^2]^2$$
$$a_{kl} = \omega_k^2/[\omega_k^2 - (l'\pi)^2]^2$$
$$f_{kl} = 1/[\omega_k^2 - (l'\pi)^2]$$
$$l' = l + 1/2, \quad \tau_k = \omega_k/2\eta, \quad \eta = h/a$$
$$\xi_l = \frac{(2-\mu)}{(l'\pi)^4} - \frac{(1-\mu)}{(l'\pi)^2}; \quad q_l = (1-\mu)/(l'\pi)^2.$$

In the equations written above, $I_n(\lambda_k r/\eta)$ with $\lambda_k = \omega_k$ or $l'\pi$ can be expressed in power series form as follows[16]:

$$I_n(\lambda_k r/\eta) = B_{nk} \sum_{m=0,1,2,}^{\infty} \frac{(\lambda_k/2\eta)^{2m} r^{n+2m}}{m!\,\phi(n,m)}$$

where

$$\phi(n,m) = (n+1)(n+2)(n+3)\ldots(n+m), \quad \text{for} \quad m \geqslant 1$$

$$\phi(n,m) = 0, \quad \text{for} \quad m = 0.$$

In the above series expansion B_{nk} are arbitrary constants which are absorbed into the unknown constants occurring in the expressions for stress and displacement components.